이학석사 학위논문

Quantitative Estimation of Conformation and Substituent Effects on the Efficiency of Photochemical Ring-Opening

광화학적 고리 열림 반응의 효율성에서의 형태 및 치환기 효과의 정량적 추정

2023 년 8 월

서울대학교 대학원
화학부 물리화학전공

임 성 민

Quantitative Estimation of Conformation and Substituent Effects on the Efficiency of Photochemical Ring-Opening

광화학적 고리 열림 반응의 효율성에서의 형태 및 치환기 효과의 정량적 추정

지도교수 정 연 준

이 논문을 이학석사 학위논문으로 제출함

2023 년 7 월

서울대학교 대학원

화학부 물리화학전공

임 성 민

임성민의 이학석사 학위논문을 인준함

2023 년 6 월

위 원 장	석 차 옥	(인)
부 위 원 장	정 연 준	(인)
위 원	김 지 환	(인)

Abstract

Photochemical ring-opening reactions are one of the most extensively employed chemical reactions in the field of chemistry. Owing to their significance, molecular-level studies of these reactions have been widely conducted. One of the major considerations in investigating the ring-opening dynamics of complex molecules on the molecular scale is the differences in dynamics between different conformers, because the number of conformers arising from a specific substrate rapidly increases with the complexity of the substrate. However, to date, studies dealing with this problem have been limited to specific individual cases. That is, a rule applicable to arbitrary conformers to estimate and explain the effects of different aspects of molecular structure, such as substituents and conformations, on photochemical ring opening has not been established. Herein, we propose the concept of *substituent-induced electron density leakage via hyperconjugation* as a candidate for this general rule. Based on our hypothesis, we present an indicator that can predict the efficiency of the photochemical ring-opening reactions of various conformers. The relative error between the ring-opening efficiency as obtained from the indicator and that obtained from the nonadiabatic simulations was less than 25% in 56 of the 66 conformers arising from 1,3-cyclohexadiene and 12 dis-

tinct analogs. This approach offers the possibility of accurately and quickly predicting the photochemical ring-opening efficiency of arbitrary molecules in arbitrary conformations.

Keywords: photochemical ring-opening, nonadiabatic molecular dynamics, natural localized molecular orbitals

Student Number: 2021-23895

Contents

List of Figures

List of Tables

Chapter 1

Introduction

Photochemical ring-opening reactions are a type of electrocyclic reaction in which a π-system on a ring is activated by light absorption, leading to the opening of the ring and the formation of a new π-bond. These reactions are commonly found in nature, such as in the production of vitamin D in human skin, and are widely used in organic synthesis, such as for the synthesis of various natural products.[1, 2] Among them, the photochemical ring-opening reaction of 1,3-cyclohexadiene (CHD) to 1,3,5-hexatriene (HT) has been extensively investigated using both experimental and computational methodologies in the molecular scale, mainly because of its simplicity. Studies have been performed on the ring opening of CHD based on spectroscopic experiments and nonadiabatic molecular dynamics (NAMD) simulations with various quantum chemical methods.[3–6]

Thanks to this interest, there is general agreement on the mechanism of this reaction (Figure 1.1).[6] CHD molecules initially in the S_0 electronic state are excited to the S_1 state by photon absorption. While they proceed on the

reaction pathway toward ring opening, some encounter the conical intersection (CI) of the nonreactive pathway (CI1 and CI2 in Figure 1.1) by folding of the CHD ring, which directs molecules into the reactant.[7, 8] Those that do not pass through CI1 and CI2 continue to proceed through S_1 to CI4. At CI4, the molecules undergo an electronic transition to S_0 and eventually become either the CHD reactant or HT product.

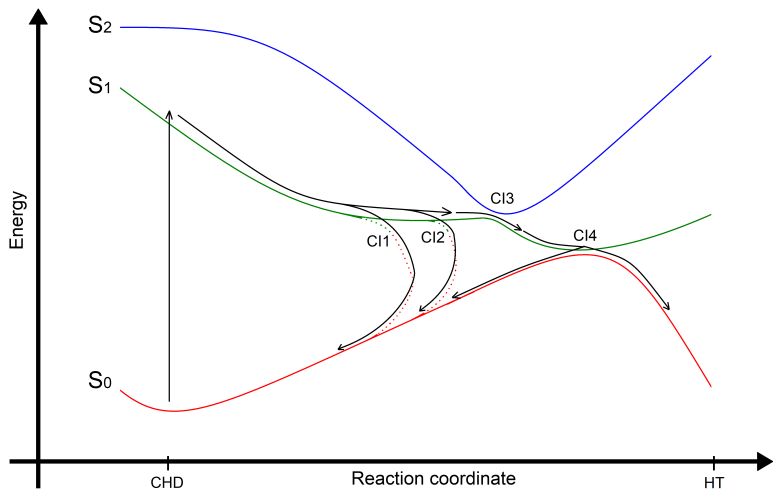

Figure 1.1: Potential energy curves for the photochemical ring opening of CHD. Black arrows represent the main reaction pathways. Red, green, and blue lines indicate the S_0, S_1, and S_2 electronic states, respectively. Dotted lines passing through CI1 and CI2 represent nonreactive pathways.

Nevertheless, as this textbook example is quite different from the photochemical ring opening of complex compounds, which are of paramount interest to chemists, understanding the dynamics of ring opening in complex cases remains a challenge. The main difficulty lies in the numerous reaction pathway bifurcations owing to various structural factors. Because of their complexity, researchers have been able to navigate the dynamics of complex molecules only recently, using novel computational techniques such as machine learning

and a newly developed time-dependent density functional theory (TDDFT)-based method.[9, 10] Although many structural factors contribute to these complex bifurcations, conformation would be one of the important elements between them. As the number of conformers derived from a specific compound rapidly increases with the complexity of the compound, understanding the differences in the ring-opening dynamics of different conformations would provide valuable insights that could be applicable to a wide range of molecules. Conformer-dependent photochemistry has been reported in a few individual cases,[11–13] but it has only recently been observed experimentally in the case of photochemical ring opening, owing to the insufficient sensitivity of past experimental methods. In that study, the quantum efficiency of the photochemical ring opening of α-Phellandrene (αPH), a CHD derivative, was reported to be conformer dependent. αPH has two major conformational isomers that have different orientations for the isopropyl (iPr) group on its sp^3-hybridized carbon in the ring: (quasi)axial and (quasi)equatorial orientations with respect to the ring plane. The results of NAMD simulations indicated that the photochemical ring-opening efficiency was higher for the αPH conformation with an equatorial iPr group than for that with an axial iPr group. In addition, this result is quantitatively consistent with observations made using ultrafast electron diffraction.[7]

However, an approach for understanding and predicting the effects of conformational differences on ring-opening efficiency in an arbitrary molecule has not yet been found. To date, studies of conformation-dependent photochemistry have been limited to specific types of molecules. Moreover, until recently, these effects have only been speculated to be explicable by something far be-

yond the Woodward–Hoffmann rules.[7, 14] These are mainly because of the very small difference in the energy barrier between different conformers of different substituents.[11] In the present paper, we propose a plausible general rule of photochemical ring opening to explain the difference in ring-opening dynamics between various conformers, termed *substituent-induced electron density leakage via hyperconjugation*. This goes beyond the results of previous studies that were based on individual molecules or types of molecules. Using our approach, we were able to calculate an indicator that predicts the efficiency of photochemical ring opening in just two steps: constrained geometry optimization of the first excited state, followed by calculation of the indicator based on the overlap between carefully selected molecular orbitals (MOs) within the optimized structure. This indicator predicted the ring-opening efficiency obtained from NAMD simulations with quantitative accuracy when tested on a total of 66 conformers arising from CHD and 12 CHD analogs. This suggests that our results are applicable to complex molecules that were not investigated in this study.

Chapter 2

Results and Discussion

2.1 Identification of Conformers and Initial Conditions

The compounds we studied were chosen from among CHD and its analogs, in which one or two hydrogen atom(s) on the sp^3-hybridized carbons of CHD were substituted. The substituents (denoted X) were selected to include a wide range of functional groups, from electron-donating to electron-withdrawing groups, while being simple enough to allow simulations to be performed in a reasonable amount of time. Selecting relatively small substituents greatly reduces steric effects, thereby enabling us to investigate the purely quantum-mechanical effects of the substituents and their conformations on the ring opening. One group of CHD analogs studied included molecules in which the hydrogen atom on the C_5 atom of CHD had been substituted (Figure 2.1a,left). In Figure 2.1a, CHD (**1**) is shown alongside its analogs in which the hydrogen atom on C_5 is substituted with CH_3, C≡CH, C≡N, NH_2, OH, and F

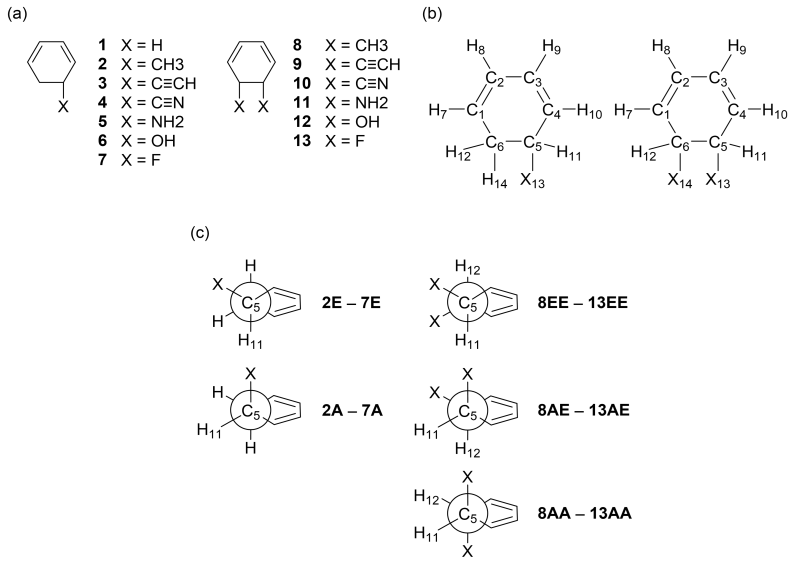

Figure 2.1: (a) CHD analogs investigated in this study. In each case, one hydrogen atom on the C_5 atom was substituted with X (left) or two hydrogen atoms—one on C_5 and one on C_6—were substituted with X (right). (b) Atom numbering in analogs **2**–**7** (left) and **8**–**13** (right). (c) Categorization of **2**–**13** based on the orientation of the X('s) with respect to the ring plane (equatorial or axial) in **2**–**7** (left) and **8**–**13** (right). For the molecules on the left, the second letter indicates the orientation of X on the C_5 atom; for the molecules on the right, the second and the third letters indicate the orientations of the X's on the C_5 and C_6 atoms, respectively.

(**2**, **3**, **4**, **5**, **6**, and **7**, respectively). The other group of CHD analogs studied consisted of molecules with two hydrogen atoms—one on C_5 and the other on C_6—substituted with the same substituent (Figure 2.1a,right). CHD analogs in which these two hydrogen atoms had been substituted with CH_3, C≡CH, C≡N, NH_2, OH, and F were selected for this study (**8**, **9**, **10**, **11**, **12**, and **13**, respectively). Conformers of analogs **2**–**13** were categorized based on the orientation of the substituent group (X) with respect to the ring plane (Figure 2.1c). The letter **E** for equatorial or **A** for axial was added after the number to the name codes for analogs **2**–**7**, depending on the orientation of X. The same

procedure was applied to analogs **8**–**13**; in these cases, however, two letters were required. As illustrated on the right of Figure 2.1c, the first and second letters added after the analog numbers **8**–**13** represent the orientation of the X substituents on the C_5 and C_6 atoms, respectively. Thus, the conformers arising from the different orientations of the X substituents in **2**–**13** were written as **2E**–**7E**, **2A**–**7A**, **8EE**–**13EE**, **8AE**–**13AE**, and **8AA**–**13AA**. Note that "**EA**" is not in this list as it is necessarily the same as "**AE**". Finally, among these, further conformations of **5E**, **5A**, **6E**, **6A**, **11EE**, **11AE**, **11AA**, **12EE**, **12AE**, and **12AA** were constructed based on the orientation of the atoms inside the substituent X. For **5E**, **5A**, **6E**, and **6A**, there are three conformers for each structure corresponding to different rotations of the bond between the C_5 atom and X_{13}. Similarly, **11AE** and **12EE** both have nine conformers each corresponding to different combinations of rotations for the two bonds C_5–X_{13} and C_6–X_{14}. However, in the cases of **11EE**, **11AA**, **12EE**, and **12AA**, although there are two rotatable bonds (C_5–X_{13} and C_6–X_{14}), three pairs of conformers were duplicates because of the C_2 symmetry of the **EE** and **AA** molecules when each of the substituents is considered as a single atom. Thus, all the conformers of **5**, **6**, **11**, and **12** are **5E1**–**5E3**, **5A1**–**5A3**, **6E1**–**6E3**, **6A1**–**6A3**, **11EE1**–**11EE6**, **11AE1**–**11AE9**, **11AA1**–**11AA6**, **12EE1**–**12EE6**, **12AE1**–**12AE9**, and **12AA1**–**12AA6**. The conformers of each analog with different orientations for X and the atoms within X, a total of 75 conformers, are summarized in Table 2.1.

Table 2.1: The number of conformers of analogs

Analog	Orientation of X	Number of conformers
1	*n/a*	1
2	**E**	1
	A	1
3	**E**	1
	A	1
4	**E**	1
	A	1
5	**E**	3
	A	3
6	**E**	3
	A	3
7	**E**	1
	A	1
8	**EE**	1
	AE	1
	AA	1
9	**EE**	1
	AE	1
	AA	1
	EE	1
10		

continued on next page

continued from previous page

Analog	Orientation of X	Number of conformers
	AE	1
	AA	1
11	**EE**	6
	AE	9
	AA	6
12	**EE**	6
	AE	9
	AA	6
13	**EE**	1
	AE	1
	AA	1

For each conformer, the ground state geometry was optimized without any constraints. After geometry optimization, 9 of the 75 conformers either converged to a different conformer or to a structure with an imaginary frequency. This occurred for one conformer of **12AA** and two conformers of **11AE**, **11AA**, **12EE**, and **12AE**. Subsequent calculations were performed for the remaining 66 conformers, excluding those with problematic convergence.

2.2 Nonadiabatic Simulation of Photochemical Ring-opening

Using the optimized structures as the initial conditions, NAMD simulations were performed using Tully's fewest switches surface hopping (FSSH) algorithm[15] and decoherence correction based on the energy difference between the electronic states.[16] For each conformer, 100 geometries and velocities were initially generated based on a Wigner distribution.[17] All the trajectories were initiated on S_1, in accordance with the generally accepted mechanism for the photochemical reaction. Although the total efficiency of ring-opening is also affected by the rate of excitation from S_0 to S_1, which is expressed in terms of the transition dipole moment between them, it was not considered here since it was out of the scope of this study. Starting from the initially excited electronic state, simulations were run for 200 fs. We assumed that a total simulation time of 200 fs would be sufficient based on two previous calculations reporting time constants for S_1 decay in CHD of 52 and 72 fs using the FSSH algorithm.[6, 18] This was further confirmed by examining the population of the electronic states of the conformers after the 200-fs simulation: at least 90% of the trajectories were in S_0 at 200 fs for 63 of the 66 conformers (the three outliers were **9AE**, **10AE**, and **10AA**). This implies that the S_1 decay timescale is much shorter than 200 fs for almost all the conformers. The electronic state populations of each of the 66 conformers are given in A.1 in the Supplementary Materials section. After 200 fs, all the trajectories were classified with respect to the bond length between C_5 and C_6, R_{56}. In this study, we categorized all the structures with $R_{56} \geq 3$

Å at 200 fs as the product; this criterion has been previously employed for determining whether a given structure is a reactant or product.[6] Using this criterion, the ring-opening efficiency of each conformer was calculated as the ratio of the number of trajectories categorized as the product at 200 fs to the total number of trajectories at 200 fs.

Figure 2.2 shows the ring-opening efficiencies of the 66 conformers; these results are tabulated in A.2 in the Supplementary Materials section. We observed that the ring-opening efficiency of the CHD analogs was dependent on the number of axially oriented X substituents across all the different types of analogs, with the efficiency generally decreasing as the number of axially oriented X substituents increased. This consistent trend over a wide range of analogs suggests the existence of general rules governing the ring-opening reaction of this entire class of molecules. In addition, this trend was in accordance with previous experimental and computational observations on the two major conformers of αPH.[7] Meanwhile, for the conformers of analogs **5**, **6**, **11**, and **12**, for which additional conformers exist owing to variations in the orientation of the atoms inside the substituents, the ring-opening efficiency differed greatly depending on the internal structure of the substituents, even among conformers with the same substituent orientation with respect to the ring plane. This indicates that the conventional functional group-based approach, in which a specific subset of atoms is considered to have similar properties irrespective of its internal structure, cannot be considered suitable for analyzing conformer-dependent photochemistry, reinforcing the need for an orbital-based approach, as discussed later.

To understand how the differences between conformers arise, we observed

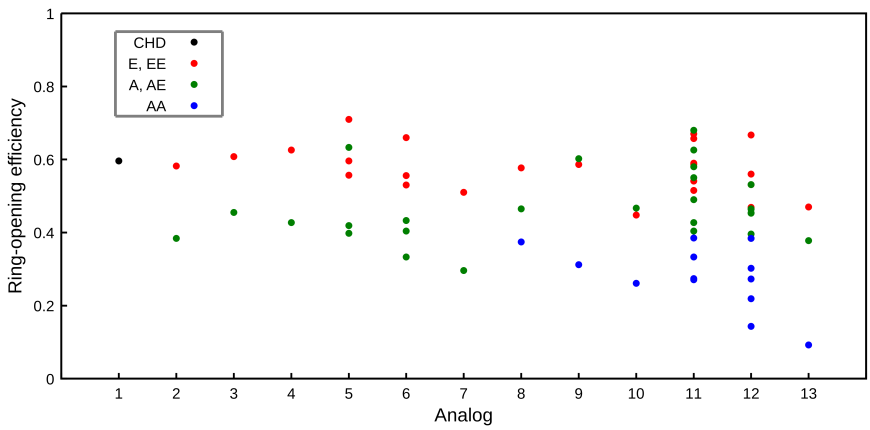

Figure 2.2: Ring-opening efficiency of each conformer obtained from NAMD simulations. On the horizontal axis, the first letter in the conformer name codes is plotted, which corresponds to the specific X substituent. The black dot indicates CHD, and red, green, and blue dots indicate conformers with zero, one, and two substituents oriented axially with respect to the ring plane, respectively.

the time dependence of the R_{56} distribution of selected conformers. In Figure 2.3, this distribution is shown for selected time points for **13EE**, **13AE**, and **13AA**. In Figure 2.3a–c, the distributions at simulation times of 0, 10, and 20 fs, respectively, are plotted. The R_{56} distribution moved toward ring opening as time evolved from (a) to (c) for each conformer; however, the extent to which this occurred decreased in the order **13EE**, **13AE**, and **13AA**. This is consistent with the differences in the ring-opening efficiencies for these conformers (analog **13** in Figure 2.2). Careful inspection of Figure 2.3 reveals that the differences in the distribution were most apparent at R_{56} values between 1.7 and 2 Å. From this result, we can infer that an energetic barrier between CHD and CI3 in the S_1 state is created by the substituents and the conformation, as shown in Figure 2.4. This barrier prevents molecules from

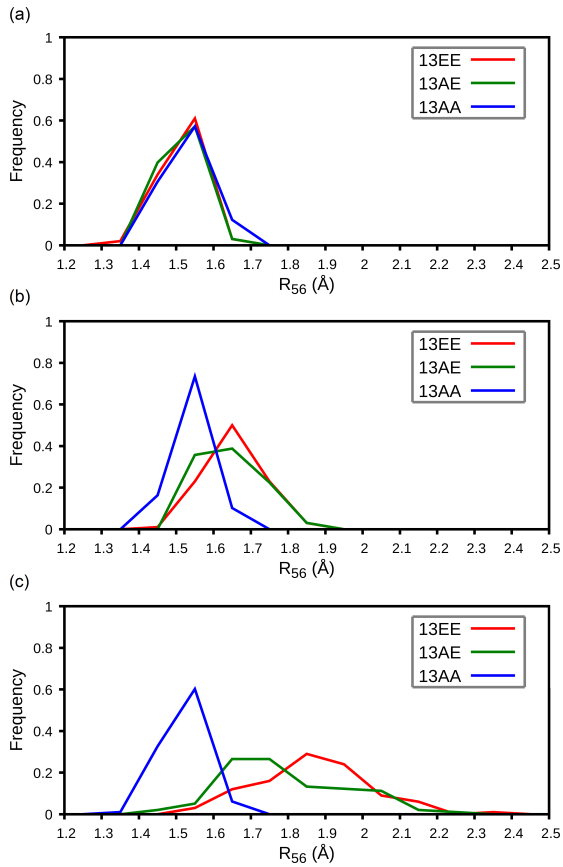

Figure 2.3: Relative frequency histogram of R_{56} for three representative conformers at (a) 0, (b) 10, and (c) 20 fs.

proceeding to CI3, thus increasing the chance of them encountering CI1 and CI2, which are gates to the unreactive pathway (Figure 1.1). This suggests that the origin of the differences in the ring-opening efficiencies of the conformers can be determined by further investigating this region of the potential energy surface.

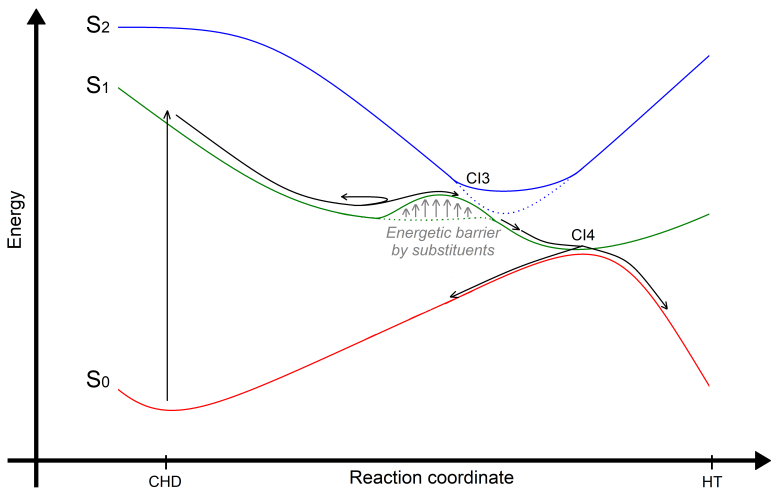

Figure 2.4: Proposed potential energy curves for the photochemical ring opening of CHD analogs; the effects of substituents and their conformations are illustrated. The dotted line represents the energy curve of the unsubstituted molecule, which is shown in Figure 1.1; note that CI1, CI2, and the nonreactive pathways in Figure 1.1 are omitted for clarity.

2.3 Obtaining an Indicator to Estimate Ring-Opening Efficiency

From the perspective of frontier molecular orbital theory,[19] elongation of R_{56} in the CHD analogs can be understood in terms of an interaction between the highest occupied molecular orbital (HOMO) of the sp^2-hybridized π-system in the first excited state and the antibonding σ^*-orbital from the sp^3-hybridized C_5–C_6 bond. This orbital interaction is illustrated in Figure 2.5(a,b), where the lowest unoccupied molecular orbital (LUMO) of the ground state in the π-system becomes the HOMO of the first excited state (Figure 2.5a), interacting with the σ^*-orbital of the sp^3-hybridized C_5–C_6 bond owing to favorable overlap and undergoing conrotatory ring opening (Figure 2.5b). Here, we hypothesized that the interaction between these two orbitals could be interrupted by hyperconjugation with the antibonding orbitals of other bonds, such as the antibonding orbitals of the C–X bond and the bonds within the substituents, as shown in Figure 2.5c. Thus, the two orbitals shown in red and blue in Figure 2.5c can be combined together to result in "leakage" of electron density originally in the π-system (Figure 2.5d). Because the antibonding orbitals inside the same molecule can be considered mutually orthogonal, this *substituent-induced electron density leakage via hyperconjugation* would decrease the intensity of the interaction shown in Figure 2.5b. In this study, we estimated that the amount of leakage a specific antibonding orbital associated with the C_5 and C_6 atoms (denoted ϕ) can cause is proportional to the square of the overlap integral, $|\langle\psi_{\mathrm{LUMO}}|\phi\rangle|^2$, where ψ_{LUMO} is the LUMO of the ground state in the sp^2-hybridized π-system. To obtain the desired

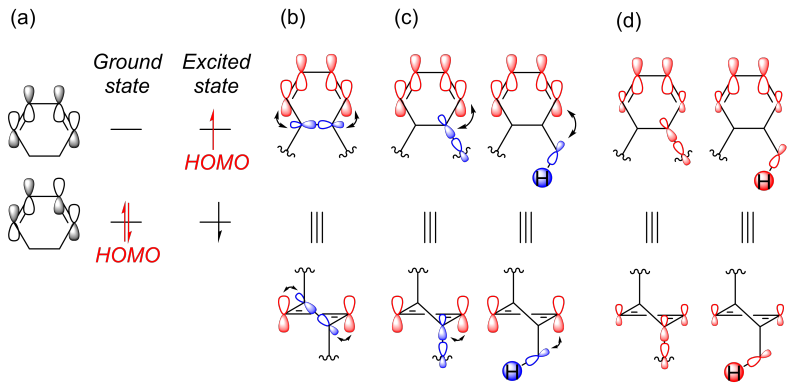

Figure 2.5: (a) Change in HOMO when CHD is excited from S_0 to S_1. (b,c) Interactions within the CHD analog based on overlap between (b) the first-excited-state HOMO and C_5–C_6 σ^*-orbital, (c, left) the HOMO of the first excited state and the antibonding orbitals of the C_5–X_{13} bond, and (c, right) the HOMO of the first excited state and bonds inside the substituent. Black arrows indicate the location of the overlap. (d) Effect of combining the two orbitals shown in (c). Leakage of the electron density in the carbon ring is indicated by the smaller p-orbitals on C_1 and C_4. In (b–d), the figures shown at the bottom are views with the ring plane perpendicular to the paper.

overlaps between orbitals within each structure, we performed a series of calculations. First, constrained geometry optimizations of the first excited states were performed for each of the 66 conformers. To measure the overlap in the region in which the deviation in ring-opening efficiency between conformers emerged (Figures 2.3 and 2.4), R_{56} was constrained to 1.85 Å. After geometry optimization, each of the 66 conformers was divided into two subsystems. The first subsystem included the carbon atoms C_1, C_2, C_3, and C_4 and the hydrogen atoms H_7, H_8, H_9, and H_{10} from the original conformer, while retaining the optimized geometry. To these atoms, two hydrogen atoms were added to the line segments C_1–C_6 and C_4–C_5 at distances of 1.08 Å from C_1 and C_4, respectively, to form a closed-shell molecular sp^2-hybridized subsystem (Figure 2.6a). Analogous to the first subsystem, the second subsystem consisted of the

carbon atoms C_5 and C_6, hydrogen atoms H_{11}, H_{12}, (and H_{14} in analogs **1**–**7**), and substituent(s) X_{13} (and X_{14} in analogs **8**–**13**) from the original conformer, also retaining the optimized geometry. Two hydrogen atoms were added to the line segments C_5–C_4 and C_6–C_1 at distances of 1.08 Å from C_5 and C_6, respectively, to form a molecular sp^3-hybridized subsystem (Figure 2.6b).

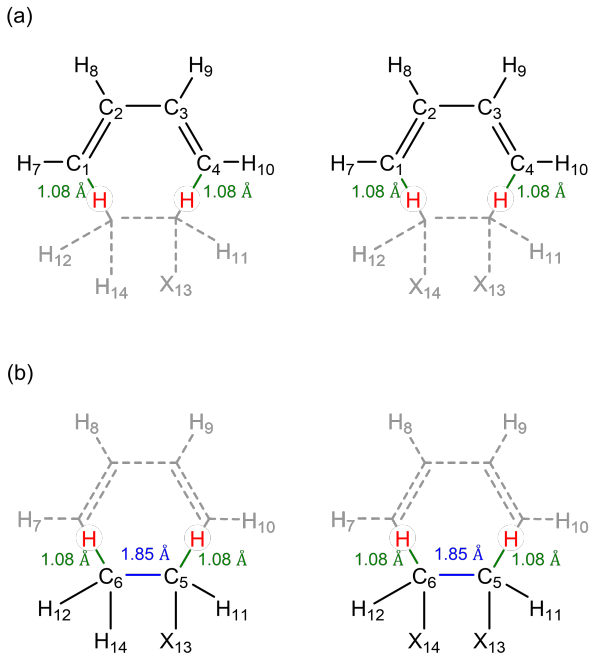

Figure 2.6: (a) sp^2-hybridized subsystem and (b) sp^3-hybridized subsystem used to obtain orbitals for overlap calculations. In (a,b), the structures on the left and right represent analogs **1**–**7** and **8**–**13**, respectively. The hydrogen atoms shown in red are those that have been placed to form closed-shell molecular subsystems. The gray dashed lines in each panel represent the atoms removed in the process of constructing the subsystems from the original molecular structure. Green and blue lines denote bonds with lengths of 1.08 and 1.85 Å, respectively.

From these two subsystems, ψ_{LUMO} and ϕ were extracted as the LUMO of the sp^2-hybridized subsystem and the virtual orbitals obtained from the valence atomic orbitals in the sp^3-hybridized subsystem, respectively. Since

information about the substituents and conformation of given conformer is delocalized over all the extracted ϕ orbitals, the amount by which the ϕ orbitals inhibit ring opening can be estimated by summing $|\langle\psi_{\mathrm{LUMO}}|\phi\rangle|^2$ over all the ϕ orbitals, i.e., $I = \sum_{\phi} |\langle\psi_{\mathrm{LUMO}}|\phi\rangle|^2$. Rather than using canonical orbitals obtained from the Hartree–Fock (HF) calculation as ϕ, using localized orbitals as ϕ allows the local interaction between ψ_{LUMO} and ϕ to be properly reflected, and better-quality results are obtained. In this study, natural localized molecular orbital (NLMO)[20] method was used to obtain localized antibonding orbitals for the sp^3-hybridized subsystem. In contrast, ψ_{LUMO} was obtained as the LUMO of the sp^2-hybridized subsystem via a standard HF calculation. The quantity I obtained in this manner can be used as an indicator to predict the ring-opening efficiency of various CHD-like molecules with different substituents and in different conformations.

Figure 2.7 shows the correlation between the ring-opening efficiency obtained from the NAMD simulations and the calculated indicator I, for the 66 conformers. The results shown in Figure 2.7 are tabulated in A.3 in the Supplementary Materials section. The correlation obtained (coefficient of determination, $R^2 = 0.607$) is consistent with our hypothesis that I increases as the ring-opening efficiency decreases. The usefulness of this indicator in terms of the relative error with respect to the efficiencies obtained from the NAMD simulations was evaluated, and it was found to be $<25\%$ for 56 of the 66 conformers. Note that because the NAMD values were subject to statistical error owing to the use of a finite number of trajectories, better performance should be demonstrable by comparing I with the results of experimental investigations of the photodynamics of the different conformers.

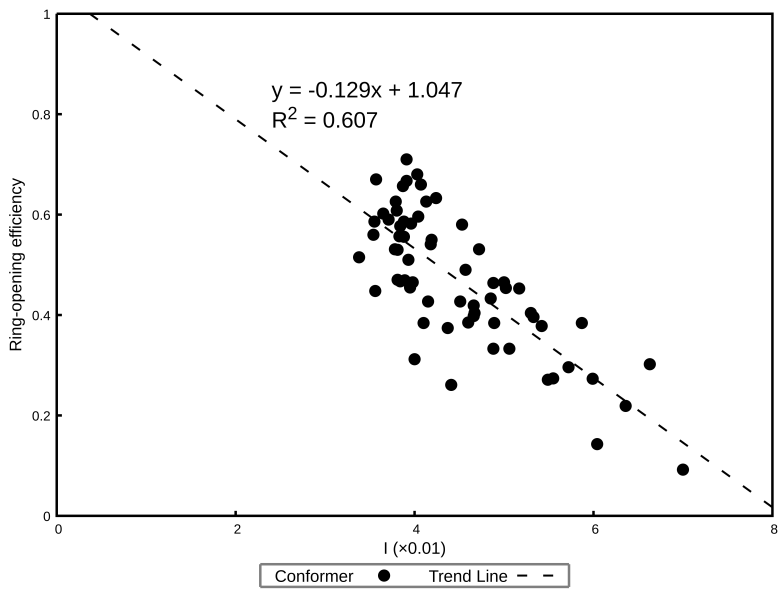

Figure 2.7: Plot of ring-opening efficiency obtained from NAMD simulations vs. calculated indicator (I).

Chapter 3

Conclusion

In this study, we demonstrated that the quantum efficiency of photochemical ring-opening reactions could be estimated by performing a constrained geometry optimization of the first excited state and calculating the overlap between the appropriate orbitals within the optimized structure. We were able to explain the effects of the substituents and conformations on the photochemical ring-opening dynamics all at once, by introducing an orbital-based approach instead of using traditional functional group-based arguments. The fact that the indicator defined in this study effectively predicted the ring-opening efficiency of 66 conformers derived from CHD and 12 other analogs containing various atoms suggests that it is applicable to a variety of molecules beyond those investigated in this study. This will enable the utilization of conformer and substituent sensitivity information in the design of photochemical ring-opening reactions across various areas of chemistry. Nonetheless, it should be emphasized that the indicator defined in this study predicted the ring-opening efficiency obtained from the NAMD simulations, not the exper-

imental efficiency. Although experimental and computational results in αPH given in the prior study[7] are consistent with the results of this study, there is currently no guarantee that this holds true for all molecules investigated in this study. We believe that additional experimental data will support the conclusions of this study. The accuracy of the computations can be increased by carefully adding parameters to be fitted; this will serve as an attractive future study for obtaining a broader understanding of conformer-dependent photochemistry.

Chapter 4

Computational Details

4.1 Quantum Chemical Calculations

Ab initio calculations required for the geometry optimization and NAMD simulations were performed using the OpenMolcas 18.09 package.[21] The state-averaged complete active space self-consistent field (SA-CASSCF) method was employed for the three lowest singlet electronic states, denoted S_0, S_1, and S_2 in ascending order of energy. Although it is common to employ complete active space second-order perturbation theory (CASPT2) or multireference configuration interaction (MRCI) together for correction, it has been reported that using SA-CASSCF alone with a clipped active space, in which only one virtual orbital is included, also gives accurate results.[6] Although whether this reduction in the level of calculation remains accurate across the entire reaction pathway is debatable, we assumed it sufficiently appropriate to elucidate differences in dynamics between conformers. This assumption was based on a study using all three methods (SA-CASSCF + CASPT2, SA-CASSCF +

MRCI, and SA-CASSCF alone with a clipped active space) that demonstrated similar tendencies for the S_1 energy of CHD and S_1 energy of CI3 (Figure 1.1), between where we observed that conformer-dependent dynamics mainly occur. [8] Since CASPT2 and MRCI are very time-consuming, using SA-CASSCF alone made it possible to perform calculations on various conformers within a reasonable amount of time. In performing the SA-CASSCF calculations, the active space of each analog was chosen to include six σ-orbitals, two π-orbitals, and a π*-orbital in the six-membered carbon ring. In addition, all the valence electrons in the substituents were included in the active space in the case of analogs with substituent(s) (see A.4 in the Supplementary Materials section for details). The 6-31G and cc-pVDZ basis sets were employed for the hydrogen and other atoms, respectively.

4.2 Geometry Optimization

Quantum chemistry-based geometry optimization was performed twice in this work: to determine the initial conditions to be used in subsequent calculations, and to obtain the desired overlaps between orbitals for the calculation of the indicator parameter to predict the photochemical ring opening efficiency. In both instances, the convergence criteria for the geometry optimization with respect to the norm of the gradient was set as 10^{-3} a.u. Conversely, while the first of these two sets of optimizations was carried out without any constraints, for the second, constraints were used to obtain optimal results. In addition to the constraints on R_{56} mentioned in the Results and Discussion section, constraints were imposed to prevent convergence into undesired structures in the second geometry optimization. The four angles between the ring plane

and the four bonds C_1–H_7, C_2–H_8, C_3–H_9, and C_4–H_{10} were constrained to the values obtained for the ground-state optimized geometry. The same constraint was applied to two angles in the ring plane: $C_1C_2C_3$ and $C_2C_3C_4$. For the conformers of analogs **5**, **6**, **11**, and **12**, for which additional conformers exist owing to variations in the orientations of atoms with the substituents, the dihedral angles defining the rotation of bonds between the ring and the substituent were constrained in the same manner. The constraints in the OpenMolcas input file format are given in A.5 in the Supplementary Materials section.

4.3 NAMD Simulations

NAMD simulations were performed using the SHARC 2.1.1 package[22, 23] interfaced with the OpenMolcas 18.09 package for the *ab initio* calculations. For each conformer, 100 geometries and velocities were initially generated based on a Wigner distribution[17], where the frequencies and normal modes of the ground state obtained from the optimized geometry, were used to generate the initial states of the trajectories. They were generated with a random seed of 19981128 and a temperature of 0 K using `wigner.py` in the SHARC 2.1.1 package. The simulations were run for 200 fs with a nuclear time step of 0.5 fs and an electronic time step of 0.02 fs. Random numbers for performing surface hopping simulations were generated with a random seed of 19981128 using the `setup_traj.py` in the SHARC 2.1.1 package. In the simulations, the maximum permissible drift of the total energy within the full trajectory, maximum permissible total energy difference between time steps, maximum permissible potential energy difference of the active state between

time steps without hopping, maximum permissible kinetic energy difference between time steps, and maximum permissible potential energy difference of the active state between time steps during hopping were set to 2.0, 1.0, 1.5, 1.5, and 5.0 eV, respectively. Trajectories violating these restrictions were excluded from subsequent analyses. Unless otherwise stated, the default settings of the package were used in the simulations.

4.4 Calculating Indicator for Estimating Ring-Opening Efficiency

The NLMOs of the sp^3-hybridized subsystems were obtained using the NLMO function implemented in the Gaussian 16 package.[24] From the obtained NLMOs, the orbitals labeled as "BD*" in the Gaussian log file, which indicates a two-center antibonding orbital, were selected to be used as ϕ for the overlap calculations. In contrast, we used the LUMO of the sp^2-hybridized subsystem obtained from standard HF calculations as ψ_{LUMO}. The overlap between the two orbitals was determined using the Multiwfn 3.8 package.[25] The basis sets employed were the same as those used for the geometry optimizations and NAMD simulations.

Appendix A

Supplementary Materials

A.1 Electronic State Populations at 200 fs of the Simulation

The table below contains number of trajectories in each electronic state and their ratio at 200 fs of the simulation, for 66 conformers investigated in this study.

Table A.1: Number of trajectories in each electronic state and their ratio after 200-fs simulation

Conformer	Number of trajectories				Ratio		
	S_0	S_1	S_2	Total	S_0	S_1	S_2
1	95	4	0	99	0.960	0.040	0.000
2E	98	0	0	98	1.000	0.000	0.000

continued on next page

continued from previous page

Conformer	Number of trajectories				Ratio		
	S_0	S_1	S_2	Total	S_0	S_1	S_2
2A	98	1	0	99	0.990	0.010	0.000
3E	94	3	0	97	0.969	0.031	0.000
3A	94	5	0	99	0.949	0.051	0.000
4E	93	5	1	99	0.939	0.051	0.010
4A	89	7	0	96	0.927	0.073	0.000
5E1	100	0	0	100	1.000	0.000	0.000
5E2	97	0	0	97	1.000	0.000	0.000
5E3	99	0	0	99	1.000	0.000	0.000
5A1	97	1	0	98	0.990	0.010	0.000
5A2	92	1	0	93	0.989	0.011	0.000
5A3	97	1	0	98	0.990	0.010	0.000
6E1	100	0	0	100	1.000	0.000	0.000
6E2	96	1	0	97	0.990	0.010	0.000
6E3	99	0	0	99	1.000	0.000	0.000
6A1	97	2	0	99	0.980	0.020	0.000
6A2	97	0	0	97	1.000	0.000	0.000
6A3	99	0	0	99	1.000	0.000	0.000
7E	95	1	0	96	0.990	0.010	0.000
7A	94	4	0	98	0.959	0.041	0.000
8EE	96	1	0	97	0.990	0.010	0.000
8AE	99	0	0	99	1.000	0.000	0.000

continued on next page

continued from previous page

Conformer	Number of trajectories				Ratio		
	S_0	S_1	S_2	Total	S_0	S_1	S_2
8AA	99	0	0	99	1.000	0.000	0.000
9EE	95	3	1	99	0.960	0.030	0.010
9AE	78	19	1	98	0.796	0.194	0.010
9AA	90	5	1	96	0.938	0.052	0.010
10EE	81	6	0	87	0.931	0.069	0.000
10AE	73	17	2	92	0.793	0.185	0.022
10AA	77	15	0	92	0.837	0.163	0.000
11EE1	100	0	0	100	1.000	0.000	0.000
11EE2	97	0	0	97	1.000	0.000	0.000
11EE3	98	1	0	99	0.990	0.010	0.000
11EE4	97	0	0	97	1.000	0.000	0.000
11EE5	99	0	0	99	1.000	0.000	0.000
11EE6	98	0	0	98	1.000	0.000	0.000
11AE1	100	0	0	100	1.000	0.000	0.000
11AE2	99	0	0	99	1.000	0.000	0.000
11AE3	100	0	0	100	1.000	0.000	0.000
11AE4	95	1	0	96	0.990	0.010	0.000
11AE5	93	1	0	94	0.989	0.011	0.000
11AE6	100	0	0	100	1.000	0.000	0.000
11AE7	95	1	0	96	0.990	0.010	0.000
11AA1	95	1	0	96	0.990	0.010	0.000

continued on next page

continued from previous page

Conformer	Number of trajectories				Ratio		
	S_0	S_1	S_2	Total	S_0	S_1	S_2
11AA2	92	1	0	93	0.989	0.011	0.000
11AA3	92	3	0	95	0.968	0.032	0.000
11AA4	95	1	0	96	0.990	0.010	0.000
12EE1	95	1	0	96	0.990	0.010	0.000
12EE2	100	0	0	100	1.000	0.000	0.000
12EE3	98	0	0	98	1.000	0.000	0.000
12EE4	99	0	0	99	1.000	0.000	0.000
12AE1	96	1	0	97	0.990	0.010	0.000
12AE2	97	0	0	97	1.000	0.000	0.000
12AE3	99	0	0	99	1.000	0.000	0.000
12AE4	99	0	0	99	1.000	0.000	0.000
12AE5	98	0	0	98	1.000	0.000	0.000
12AE6	90	1	0	91	0.989	0.011	0.000
12AE7	95	0	0	95	1.000	0.000	0.000
12AA1	97	1	0	98	0.990	0.010	0.000
12AA2	97	1	1	99	0.980	0.010	0.010
12AA3	94	5	0	99	0.949	0.051	0.000
12AA4	96	0	0	96	1.000	0.000	0.000
12AA5	95	1	0	96	0.990	0.010	0.000
13EE	98	2	0	100	0.980	0.020	0.000
13AE	93	5	0	98	0.949	0.051	0.000

continued on next page

continued from previous page

Conformer	Number of trajectories				Ratio		
	S_0	S_1	S_2	Total	S_0	S_1	S_2
13AA	95	3	0	98	0.969	0.031	0.000

100 trajectories containing geometries and velocities were initially generated for each conformer. The disparity between the total number of initially generated trajectories and the sum of the number of trajectories in three electronic states at 200 fs is caused by trajectories which are stopped while running simulation due to internal errors of the package or excluded for violating energy restrictions mentioned in Computational Details section of the main text. Each of ratio has been rounded to three decimal places.

A.2 Tabulated Ring-Opening Efficiencies

The table below contains ring-opening efficiencies of each conformer shown in Figure 2.2 of the main text. They were calculated as the ratio of the number of trajectories categorized as the product at 200 fs to the total number of trajectories at 200 fs.

Table A.2: Ring-opening efficiencies of each conformer obtained from NAMD simulations

Conformer	Number of trajectories			Ring-opening efficiency
	Product	Reactant	Total	
1	59	40	99	0.596
2E	57	41	98	0.582
2A	38	61	99	0.384
3E	59	38	97	0.608
3A	45	54	99	0.455
4E	62	37	99	0.626
4A	41	55	96	0.427
5E1	71	29	100	0.710
5E2	54	43	97	0.557
5E3	59	40	99	0.596
5A1	62	36	98	0.633
5A2	39	54	93	0.419

continued on next page

continued from previous page

Conformer	Number of trajectories			Ring-opening efficiency
	Product	Reactant	Total	
5A3	39	59	98	0.398
6E1	53	47	100	0.530
6E2	64	33	97	0.660
6E3	55	44	99	0.556
6A1	33	66	99	0.333
6A2	42	55	97	0.433
6A3	40	59	99	0.404
7E	49	47	96	0.510
7A	29	69	98	0.296
8EE	56	41	97	0.577
8AE	46	53	99	0.465
8AA	37	62	99	0.374
9EE	58	41	99	0.586
9AE	59	39	98	0.602
9AA	30	66	96	0.312
10EE	39	48	87	0.448
10AE	43	49	92	0.467
10AA	24	68	92	0.261
11EE1	59	41	100	0.590
11EE2	65	32	97	0.670
11EE3	65	34	99	0.657

continued on next page

continued from previous page

Conformer	Number of trajectories			Ring-opening efficiency
	Product	Reactant	Total	
11EE4	50	47	97	0.515
11EE5	58	41	99	0.586
11EE6	53	45	98	0.541
11AE1	68	32	100	0.680
11AE2	62	37	99	0.626
11AE3	55	45	100	0.550
11AE4	41	55	96	0.427
11AE5	38	56	94	0.404
11AE6	58	42	100	0.580
11AE7	47	49	96	0.490
11AA1	37	59	96	0.385
11AA2	31	62	93	0.333
11AA3	26	69	95	0.274
11AA4	26	70	96	0.271
12EE1	51	45	96	0.531
12EE2	56	44	100	0.560
12EE3	46	52	98	0.469
12EE4	66	33	99	0.667
12AE1	45	52	97	0.464
12AE2	44	53	97	0.454
12AE3	38	61	99	0.384

continued on next page

continued from previous page

Conformer	Number of trajectories			Ring-opening efficiency
	Product	Reactant	Total	
12AE4	46	53	99	0.465
12AE5	52	46	98	0.531
12AE6	36	55	91	0.396
12AE7	43	52	95	0.453
12AA1	14	84	98	0.143
12AA2	27	72	99	0.273
12AA3	38	61	99	0.384
12AA4	21	75	96	0.219
12AA5	29	67	96	0.302
13EE	47	53	100	0.470
13AE	37	61	98	0.378
13AA	9	89	98	0.092

100 trajectories containing geometries and velocities were initially generated for each conformer. The disparity between the total number of initially generated trajectories and the sum of the number of trajectories categorized as the product and the reactant at 200 fs is caused by trajectories which are stopped while running simulation due to internal errors of the package or excluded for violating energy restrictions mentioned in Computational Details section of the main text. Each of efficiency has been rounded to three decimal places.

A.3 Tabulated Indicator of Ring-Opening Efficiency

The table below contains calculated indicator (denoted I) and corresponding ring-opening efficiency of each conformer shown in Figure 2.7 of the main text.

Table A.3: Calculated indicator and the ring-opening efficiency of each conformer

Conformer	I ($\times 0.01$)	Ring-opening efficiency
1	4.04	0.596
2E	3.96	0.582
2A	4.10	0.384
3E	3.80	0.608
3A	3.95	0.455
4E	3.79	0.626
4A	4.15	0.427
5E1	3.91	0.710
5E2	3.83	0.557
5E3	4.04	0.596
5A1	4.24	0.633
5A2	4.66	0.419
5A3	4.66	0.398
6E1	3.81	0.530

continued on next page

continued from previous page

Conformer	I ($\times 0.01$)	Ring-opening efficiency
6E2	4.07	0.660
6E3	3.88	0.556
6A1	4.88	0.333
6A2	4.85	0.433
6A3	5.30	0.404
7E	3.93	0.510
7A	5.72	0.296
8EE	3.84	0.577
8AE	3.98	0.465
8AA	4.37	0.374
9EE	3.55	0.586
9AE	3.65	0.602
9AA	4.00	0.312
10EE	3.56	0.448
10AE	3.84	0.467
10AA	4.41	0.261
11EE1	3.71	0.590
11EE2	3.57	0.670
11EE3	3.87	0.657
11EE4	3.38	0.515
11EE5	3.88	0.586
11EE6	4.18	0.541

continued on next page

continued from previous page

Conformer	I ($\times 0.01$)	Ring-opening efficiency
11AE1	4.03	0.680
11AE2	4.13	0.626
11AE3	4.19	0.550
11AE4	4.51	0.427
11AE5	4.67	0.404
11AE6	4.53	0.580
11AE7	4.57	0.490
11AA1	4.60	0.385
11AA2	5.06	0.333
11AA3	5.55	0.274
11AA4	5.49	0.271
12EE1	3.78	0.531
12EE2	3.54	0.560
12EE3	3.89	0.469
12EE4	3.91	0.667
12AE1	4.88	0.464
12AE2	5.02	0.454
12AE3	4.89	0.384
12AE4	5.00	0.465
12AE5	4.72	0.531
12AE6	5.33	0.396
12AE7	5.17	0.453

continued on next page

continued from previous page

Conformer	I ($\times 0.01$)	Ring-opening efficiency
12AA1	6.04	0.143
12AA2	5.99	0.273
12AA3	5.87	0.384
12AA4	6.36	0.219
12AA5	6.63	0.302
13EE	3.81	0.470
13AE	5.42	0.378
13AA	7.00	0.092

Each value shown above is calculated by multiplying the originally calculated indicator by 100 and rounding to two decimal places. Each efficiency was rounded to three decimal places.

A.4 Active Space of Each Analog in SA-CASSCF Calculations

The table below contains the active space of confomers of each analog in performing SA-CASSCF calculations. For instance, the active space of (16e, 9o) for analog **1** denotes that 16 active electrons are contained in 9 active orbitals.

Table A.4: Active space of each analog in performing SA-CASSCF calculations

Analog	Active space
1	(16e, 9o)
2	(24e, 13o)
3	(26e, 14o)
4	(26e, 14o)
5	(24e, 13o)
6	(24e, 13o)
7	(24e, 13o)
8	(32e, 17o)
9	(36e, 19o)
10	(36e, 19o)
11	(32e, 17o)
12	(32e, 17o)

continued on next page

continued from previous page

Analog	Active space
13	(32e, 17o)

A.5 Format of Constraints in OpenMolcas Input File

Shown below is an expression of all constraints imposed to conformers of analog **5** in OpenMolcas input format.

```
&GATEWAY
...
Constraints
r_1 = Bond C5 C6
op1_1 = OutOfP H7 C6 C2 C1
op1_2 = OutOfP H8 C1 C3 C2
op1_3 = OutOfP H9 C2 C4 C3
op1_4 = OutOfP H10 C3 C5 C4
a1_1 = Angle C1 C2 C3
a1_2 = Angle C2 C3 C4
d2_1 = Dihedral H11 C5 N13 H15
d2_2 = Dihedral H11 C5 N13 H16
Values
r_1 = 1.85 Angstrom
op1_1 = fix
op1_2 = fix
op1_3 = fix
op1_4 = fix
a1_1 = fix
a1_2 = fix
d2_1 = fix
```

```
d2_2 = fix
End of constraints
...
```

In the OpenMolcas input file, constraints mentioned in the main text are expressed as lines of keywords. The table below contains descriptions of them.

Table A.5: Description of constraints expressed as keywords

Keyword	Description
Bond A B	Length between the atom A and the atom B
OutOfP A B C D	Angle between the plane BCD and the line AD
Angle A B C	Angle between the line AB and the line BC
Dihedral A B C D	Angle between the plane ABC and the plane BCD

Using the keywords above, constraints imposed to the other conformers can be expressed in the same manner.

Bibliography

(1) Havinga, E.; Schlatmann, J. *Tetrahedron* **1961**, *16*, 146–152, DOI: 10.1016/0040-4020(61)80065-3.

(2) Bach, T.; Hehn, J. P. *Angew. Chem. Int. Ed.* **2011**, *50*, 1000–1045, DOI: 10.1002/anie.201002845.

(3) Deb, S.; Weber, P. *Annu. Rev. Phys. Chem.* **2011**, *62*, 19–39, DOI: 10.1146/annurev.physchem.012809.103350.

(4) Travnikova, O.; Piteša, T.; Ponzi, A.; Sapunar, M.; Squibb, R. J.; Richter, R.; Finetti, P.; Fraia, M. D.; Fanis, A. D.; Mahne, N.; Manfredda, M.; Zhaunerchyk, V.; Marchenko, T.; Guillemin, R.; Journel, L.; Prince, K. C.; Callegari, C.; Simon, M.; Feifel, R.; Decleva, P.; Došlić, N.; Piancastelli, M. N. *J. Am. Chem. Soc.* **2022**, *144*, 21878–21886, DOI: 10.1021/jacs.2c06296.

(5) Arruda, B. C.; Sension, R. J. *Phys. Chem. Chem. Phys.* **2014**, *16*, 4439–4455, DOI: 10.1039/c3cp54767a.

(6) Polyak, I.; Hutton, L.; Crespo-Otero, R.; Barbatti, M.; Knowles, P. J. *J. Chem. Theory Comput.* **2019**, *15*, 3929–3940, DOI: 10.1021/acs.jctc.9b00396.

(7) Champenois, E. G.; Sanchez, D. M.; Yang, J.; Rodrigues, O.; Attar, A.; Centurion, M.; Forbes, R.; Gühr, M.; Hegazy, K.; Ji, F.; Saha, S. K.; Liu, Y.; Lin, M.-F.; Luo, D.; Moore, B.; Shen, X.; Ware, M. R.; Wang, X. J.; Martínez, T. J.; Wolf, T. J. A. *Science* **2021**, *374*, 178–182, DOI: 10.1126/science.abk3132.

(8) Lei, Y.; Wu, H.; Zheng, X.-l.; Zhai, G.; Zhu, C. *J. Photochem. Photobiol. A* **2016**, *317*, 39–49, DOI: 10.1016/j.jphotochem.2015.10.025.

(9) Li, J.; Stein, R.; Adrion, D. M.; Lopez, S. A. *J. Am. Chem. Soc.* **2021**, *143*, 20166–20175, DOI: 10.1021/jacs.1c07725.

(10) Shostak, S. N.; Park, W.; Oh, J.; Kim, J.; Lee, S.; Nam, H.; Filatov, M.; Kim, D.; Choi, C. H. *J. Am. Chem. Soc.* **2023**, *145*, 1638–1648, DOI: 10.1021/jacs.2c09800.

(11) Kim, M. H.; Shen, L.; Tao, H.; Martinez, T. J.; Suits, A. G. *Science* **2007**, *315*, 1561–1565, DOI: 10.1126/science.1136453.

(12) Park, S. T.; Kim, S. K.; Kim, M. S. *Nature* **2002**, *415*, 306–308, DOI: 10.1038/415306a.

(13) Choi, K.-W.; Ahn, D.-S.; Lee, J.-H.; Kim, S. K. *Chem. Commun.* **2007**, 1041–1043, DOI: 10.1039/b613011a.

(14) Woodward, R. B.; Hoffmann, R. *Angew. Chem. Int. Ed.* **1969**, *8*, 781–853, DOI: 10.1002/anie.196907811.

(15) Tully, J. C. *J. Chem. Phys.* **1990**, *93*, 1061–1071, DOI: 10.1063/1.459170.

(16) Granucci, G.; Persico, M.; Zoccante, A. *J. Chem. Phys.* **2010**, *133*, 134111, DOI: 10.1063/1.3489004.

(17) Wigner, E. *Phys. Rev.* **1932**, *40*, 749–759, DOI: 10.1103/physrev.40.749.

(18) Schalk, O.; Geng, T.; Thompson, T.; Baluyot, N.; Thomas, R. D.; Tapavicza, E.; Hansson, T. *J. Phys. Chem. A* **2016**, *120*, 2320–2329, DOI: 10.1021/acs.jpca.5b10928.

(19) Fukui, K.; Yonezawa, T.; Shingu, H. *J. Chem. Phys.* **1952**, *20*, 722–725, DOI: 10.1063/1.1700523.

(20) Reed, A. E.; Weinhold, F. *J. Chem. Phys.* **1985**, *83*, 1736–1740, DOI: 10.1063/1.449360.

(21) Fdez. Galván, I.; Vacher, M.; Alavi, A.; Angeli, C.; Aquilante, F.; Autschbach, J.; Bao, J. J.; Bokarev, S. I.; Bogdanov, N. A.; Carlson, R. K.; Chibotaru, L. F.; Creutzberg, J.; Dattani, N.; Delcey, M. G.; Dong, S. S.; Dreuw, A.; Freitag, L.; Frutos, L. M.; Gagliardi, L.; Gendron, F.; Giussani, A.; González, L.; Grell, G.; Guo, M.; Hoyer, C. E.; Johansson, M.; Keller, S.; Knecht, S.; Kovačević, G.; Källman, E.; Li Manni, G.; Lundberg, M.; Ma, Y.; Mai, S.; Malhado, J. P.; Malmqvist, P. Å.; Marquetand, P.; Mewes, S. A.; Norell, J.; Olivucci, M.; Oppel, M.; Phung, Q. M.; Pierloot, K.; Plasser, F.; Reiher, M.; Sand, A. M.; Schapiro, I.; Sharma, P.; Stein, C. J.; Sørensen, L. K.; Truhlar, D. G.; Ugandi, M.; Ungur, L.; Valentini, A.; Vancoillie, S.; Veryazov, V.; Weser, O.; Wesołowski, T. A.; Widmark, P.-O.; Wouters, S.; Zech, A.; Zobel, J. P.; Lindh, R. *J. Chem. Theory Comput.* **2019**, *15*, 5925–5964, DOI: 10.1021/acs.jctc.9b00532.

(22) Richter, M.; Marquetand, P.; González-Vázquez, J.; Sola, I. R.; González, L. *J. Chem. Theory Comput.* **2011**, *7*, 1253–1258, DOI: 10.1021/ct1007394.

(23) Mai, S.; Marquetand, P.; González, L. *Wiley Interdiscip. Rev. Comput. Mol. Sci.* **2018**, *8*, DOI: 10.1002/wcms.1370.

(24) Frisch, M. J.; Trucks, G. W.; Schlegel, H. B.; Scuseria, G. E.; Robb, M. A.; Cheeseman, J. R.; Scalmani, G.; Barone, V.; Petersson, G. A.; Nakatsuji, H.; Li, X.; Caricato, M.; Marenich, A. V.; Bloino, J.; Janesko, B. G.; Gomperts, R.; Mennucci, B.; Hratchian, H. P.; Ortiz, J. V.; Izmaylov, A. F.; Sonnenberg, J. L.; Williams-Young, D.; Ding, F.; Lipparini, F.; Egidi, F.; Goings, J.; Peng, B.; Petrone, A.; Henderson, T.; Ranasinghe, D.; Zakrzewski, V. G.; Gao, J.; Rega, N.; Zheng, G.; Liang, W.; Hada, M.; Ehara, M.; Toyota, K.; Fukuda, R.; Hasegawa, J.; Ishida, M.; Nakajima, T.; Honda, Y.; Kitao, O.; Nakai, H.; Vreven, T.; Throssell, K.; Montgomery Jr., J. A.; Peralta, J. E.; Ogliaro, F.; Bearpark, M. J.; Heyd, J. J.; Brothers, E. N.; Kudin, K. N.; Staroverov, V. N.; Keith, T. A.; Kobayashi, R.; Normand, J.; Raghavachari, K.; Rendell, A. P.; Burant, J. C.; Iyengar, S. S.; Tomasi, J.; Cossi, M.; Millam, J. M.; Klene, M.; Adamo, C.; Cammi, R.; Ochterski, J. W.; Martin, R. L.; Morokuma, K.; Farkas, O.; Foresman, J. B.; Fox, D. J. Gaussian16 Revision C.01, Gaussian Inc. Wallingford CT, 2016.

(25) Lu, T.; Chen, F. *J. Comput. Chem.* **2012**, *33*, 580–592, DOI: 10.1002/jcc.22885.

국문 초록

광화학적 고리 열림 반응은 화학 분야에서 가장 널리 사용되는 화학 반응 중 하나이다. 그 중요성 때문에, 이는 이론적 접근과 실험적 접근법 모두를 통해 널리 연구되어 왔다. 분자가 복잡해질수록 그 분자가 가질 수 있는 형태의 개수가 빠르게 증가하기 때문에, 여러 복잡한 분자들의 광화학적 고리 열림 반응을 연구하기 위해서는 각 분자의 반응이 개시되는 시점의 형태가 특히 중요해진다. 그러나, 지금까지 분자 규모에서 이를 다루는 많은 연구들과 보고들은 몇몇 가지의 특정한 분자에 한정되어 있었다. 이는 분자에 존재하는 치환기와 그 형태와 같은 분자 구조의 차이로 인해 생하는 에너지 차이가 매우 작기 때문에 이로 인한 광화학적 고리 열림 반응에 끼치는 영향을 일반적인 경우에서 측정할 수 있는 도구가 알려져 있지 않기 때문이다. 본 연구에서는 '치환기의 하이퍼컨쥬게이션에 의한 전자 밀도 누출'로 명명한 치환기와 그 형태 등의 분자 구조가 고리 열림 반응의 동역학에 미치는 영향을 설명할 수 있는 가설을 제시하였다. 또한, 이 가설을 바탕으로 다양한 치환기와 형태를 가지는 분자들의 광화학적 고리 열림 반응의 효율을 예측할 수 있는 표지자를 제시하였다. 1,3-사이클로헥사다이엔과 그 12개의 유도체에서 얻은 66개의 분자 구조에 대해 본 연구에서 얻은 표지자의 효용성을 시험하였을 때, 해당 표지자는 66개의 분자 구조 중 56개에 대해 25% 미만의 오차율로 제일원리 비단열 분자동역학 시뮬레이션에서 얻은 고리 열림 반응의 효율을 예측할 수 있었다. 이는 본 연구에서 직접적으로 다루지 않은 임의의 분자,

임의의 형태의 분자들에서도 광화학적 고리 열림 효율을 정확하고 빠르게 예측할 수 있음을 시사한다.

주요어: 광화학적 고리 열림, 제일원리 비단열 분자동역학, 국소화 분자 궤도 함수
학번: 2021-23895

감사의 글

2년 반 동안의 석사 학위 과정의 결실을 이제 맺고자 합니다. 비록 화학 연구자로서 필요한 자질을 전부 배우기에는 부족한 시간이었지만, 대학원 입학 당시만 해도 연구 활동을 전혀 경험해보지 못했던 제가 학위 과정 동안 성장할 수 있도록 도움을 주신 분들에 대한 감사의 인사를 이 글을 통해 드리고자 합니다.

먼저, 석사 학위 기간 동안 물심양면으로 많은 지원을 해 주신 정연준 지도교수님께 제 고마움을 표합니다. 학위 과정 중에 해 주신 많은 조언과 가르침을 통해 계산화학에 대한 저의 안목을 넓히고 화학자로서의 첫 걸음을 성공적으로 내딛을 수 있었습니다.

바쁘신 중에 졸업 논문 심사에 참석해주신 석차옥 교수님, 김지환 교수님께 감사드립니다. 서로의 연구에 대한 깊은 논의를 같이 진행하였던 저희 연구실의 모든 전, 현 연구원분들께도 감사의 말씀을 드립니다.

마지막으로, 먼 곳에서 든든히 응원해 주신 부모님과 가족들의 은혜를 언제나 기억하겠습니다.